Biomaterials 74 (2016) 144–154

Contents lists available at ScienceDirect

Biomaterials

journal homepage: www.elsevier.com/locate/biomaterials

Small gold nanorods laden macrophages for enhanced tumor coverage in photothermal therapy

Zhibin Li [a], Hao Huang [a], Siying Tang [a], Yong Li [a], Xue-Feng Yu [a, *], Huaiyu Wang [a, b], Penghui Li [a, b], Zhengbo Sun [a, c], Han Zhang [c], Chenli Liu [a], Paul K. Chu [b, **]

[a] Institute of Biomedicine and Biotechnology, Shenzhen Institutes of Advanced Technology, Chinese Academy of Sciences, Shenzhen 518055, Guangdong, PR China
[b] Department of Physics and Materials Science, City University of Hong Kong, Tat Chee Avenue, Kowloon, Hong Kong
[c] SZU-NUS Collaborative Innovation Center for Optoelectronic Science and Technology, Key Laboratory of Optoelectronic Devices and Systems of Ministry of Education and Guangdong Province, College of Optoelectronic Engineering, Shenzhen University, Shenzhen 518060, Guangdong, PR China

ARTICLE INFO

Article history:
Received 2 July 2015
Received in revised form
25 September 2015
Accepted 26 September 2015
Available online 30 September 2015

Keywords:
Photothermal therapy
Gold nanorods
Macrophages
Nanoparticle delivery
Tumors

ABSTRACT

One of the challenges to adopt photothermal ablation clinically is optimization of the agent delivery *in vivo*. Herein, a cell-mediated delivery and therapy system by employing macrophage vehicles to transport 7 nm diameter Au nanorods (sAuNRs) is described. Owing to the small size, the sAuNRs exhibit much higher macrophage uptake and negligible cytotoxicity in comparison with commonly used 14 nm diameter AuNRs to achieve healthy BSA-coated sAuNRs-laden-macrophages. By delivering BSA-coated sAuNRs to the entire tumor after intratumoral injection, the BSA-coated sAuNRs-laden-macrophages show greatly improved photothermal conversion almost everywhere in the tumor, resulting in minimized tumor recurrence rates compared to free BSA-coated sAuNRs. Our findings not only provide a desirable approach to improve the photothermal therapy efficiency by optimizing the intratumoral distribution of the agents, but also expedite clinical application of nanotechnology to cancer treatment.

1. Introduction

Nanomaterials-mediated photothermal therapy (PTT) using near-infrared (NIR) light is a promising strategy in cancer treatment [1]. This type of light-triggered treatment modality has improved selectivity and fewer side effects than conventional radiotherapies and chemotherapies [2,3]. In PTT, NIR light (for example, ~800 nm) is absorbed by the agent to create local hyperthermia leading to tumor cell death [4]. To minimize tumor recurrence, efficient delivery of the agent to the entire tumor region is critical in order to ensure cytotoxic temperature everywhere in the tumor [5]. So far, various types of nanoparticles have been used as photothermal agents in cancer treatment [2,3,6–20]. In general, nanoparticles *via* injection are believed to target tumors by passive (for example, by enhanced permeability and retention (EPR) effect) [6,9,11,12] and/or active (for example, ligand-mediated) targeting [8,11,14]. However, the injected nanoparticles tend to accumulate in the EPR organs such as the liver and spleen and there may be long-term harmful effects [21]. Furthermore, virtually all molecular or nanoparticle-based therapies are inaccessible to the hypoxic areas of tumors that lack blood flow thus limiting the treatment efficacy [13]. Direct intratumoral injection can be used to circumvent the inefficiency and off-target deposition has been observed from intravenous administration [22,23]. However, the injected nanoparticles generally remain at the site of injection and are unable to penetrate the tumor mass leading to incomplete ablation and disease recurrence. Hence, it is highly desirable to develop a new delivery system to improve agent delivery *in vivo* and enhancing the PTT efficiency.

Cell-mediated delivery of drugs or nanoparticles has large potential in cancer therapy because they can cross the nearly impermeable biological barriers to reach many areas in the body that common drugs/nanoparticles cannot normally access [24–29]. In recent years, cell-mediated delivery has been widely used in the therapy of many kinds of tumors, including glioma, head and neck carcinoma, breast cancer and so on [30–32]. Based on the mechanism, this method appears to be suitable for all kinds of tumors [30] but in reality, not all cells can be treated by cell delivery. In general,

* Corresponding author.
** Corresponding author.
E-mail addresses: xf.yu@siat.ac.cn (X.-F. Yu), paul.chu@cityu.edu.hk (P.K. Chu).

http://dx.doi.org/10.1016/j.biomaterials.2015.09.038
0142-9612/

the cells should have a high loading capacity for the drugs or nanomaterials and have the target tumor ability, for example, monocytes/macrophages, mesenchymal stem cell [31], and neural stem cell [32]. Typically, monocytes/macrophages are attractive nanoparticle delivery vehicles because they are circulating cells which can be easily obtained from patients [33,34]. Moreover, macrophages can be readily loaded with therapeutic nanoparticles based on the innate phagocytotic capability and each cell can serve as a "Trojan Horse" delivery vector to reach otherwise inaccessible tumor regions including the hypoxic areas [24–26]. It has been reported that Au nanoshells endocytosed by macrophages maintain the photothermal performance and the loaded cells can infiltrate tumor spheroids [24] and Au nanoshells loaded macrophages can migrate into glioma cancer cell spheroids to produce therapeutic effects in photothermal treatment [25]. Although these studies reveal efficient migration and therapeutic efficacy of macrophages carrying Au nanoshells *in vitro*, the *in vivo* PTT efficacy of the nanoparticles laden macrophages has not been demonstrated. As aforementioned, the efficacy of PTT depends on the agent concentration in the targeted tissue and development of a healthy macrophage-nanoparticle system with high nanoparticle uptake is crucial to efficient delivery and therapy *in vivo*.

Although many kinds of photothermal nanoparticles have been developed, Au nanostructures are particularly appealing because of their low toxicity and ease of biomolecule conjugation [2,35,36]. Among the various Au nanostructures, Au nanorods (AuNRs) have aroused recent biomedical interest on account of their unique surface plasmon resonance (SPR) band in the NIR region [37–44]. Owing to the characteristic longitudinal SPR (LSPR) band, AuNRs have a larger NIR absorption cross section than other Au nanostructures such as Au nanoshells which have been studied in clinical trials [45]. It has also been reported that AuNRs heat up at least 6 times faster than Au nanoshells on a per gram basis [2,46]. In addition to the photothermal performance, the particle size is also crucial to cell delivery because it influences the cell uptake and biocompatibility [47,48]. Because of the size limitation of endocytosis, smaller nanoparticles generally show higher cell uptake. The commonly used AuNRs with the LSPR peak at ~800 nm are typically about 14 nm in diameter and about 50 nm long [49,50]. Further decrease in the AuNR size can improve cell uptake and delivery but it is difficult due to the limitation in the common seed-mediated method. In this study, a one-"spot" seedless method is developed to synthesize 7 nm diameter AuNRs (designated sAuNRs) which enable efficient cell uptake in cell-mediated PTT applications. Compared to the more common 14 nm diameter AuNRs (designated bAuNRs), the sAuNRs have similar SPR bands and photothermal properties but better biocompatibility and higher cell uptake to macrophages. The sAuNRs laden macrophages are investigated *in intro* and *in vivo* to demonstrate their capability to improve the distribution of sAuNRs in tumors to enhance the PTT efficiency.

2. Experiments details

2.1. Synthesis and characterization of AuNRs

2.1.1. Materials

Chloroauric acid ($HAuCl_4 \cdot 4H_2O$, 99.99%), silver nitrate ($AgNO_3$, 99.8%), L-ascorbic acid (AA, 99.7%), NaOL, and hydrochloric acid (HCl, 36–38%) were purchased from Sinopharm Chemical Reagent Co. Ltd. (Shanghai, China), sodium borohydride ($NaBH_4$, 96%), were obtained from Aldrich (USA), and hexadecyltrimethylammonium bromide (CTAB, 99.0%) was purchased from Amresco Inc. (USA). All the chemicals were used as received without purification. Ultrapure water with a resistivity of 18.25 MΩ cm was used as the solvent in all the experiments.

2.1.2. Synthesis of AuNRs

The sAuNRs were synthesized by a one-pot seedless technique. Typically, 1 mL of 5 mM $HAuCl_4$, 5 mL of 0.2 M CTAB, and 4.5 mL of ultrapure water were mixed in a 50 mL glass beaker and then 500 μL of 0.1 M NaOL and 250 μL of 4 mM $AgNO_3$ were added under gentle stirring. Afterwards, 8 μL of concentrated HCl (36%–38%) were injected, followed by addition of 56 μL of 0.1 M ascorbic acid under slight swirling until the solution changed from dark orange to colorless. 15 μL of freshly prepared ice-cold 10 mM of $NaBH_4$ were added rapidly. The solution was gently mixed for 10 s and left undisturbed for 3 h in an incubator at 35 °C. The nanorod solution was centrifuged at 16,000 rpm for 15 min to stop the reaction. The supernatant was removed and the precipitate was re-suspended in ultrapure water. In comparison, the bAuNRs were synthesized by a common seed-mediated method in CTAB solutions as reported previously [43].

2.1.3. BSA conjugation

Bovine serum albumin (BSA) was used to conjugate with the AuNRs based on the method described by Moustafa et al. [51]. The BSA was dissolved in the phosphate-buffered saline (PBS: 150 mM NaCl, 1.9 mM NaH_2PO_4, 8.1 mM Na_2HPO_4, pH of 7.4) at a concentration of 0.25 mM. 1 mL of the 0.25 mM BSA was added to 10 mL of the AuNR solution (0.3 nM) and stirred vigorously for 8 h at room temperature. Afterwards, the reaction was stopped by removing the excess BSA by centrifugation at 10,000 rpm for 5 min and the precipitate was re-suspended in ultrapure water.

2.1.4. Characterization

Transmission electron microscopy (TEM) was performed on a JEOL 2010 (HT) TEM at an accelerating voltage of 200 kV. Absorption spectra were acquired on a Lambda 750 UV-VIS-NIR spectrometer (PerkinElmer, USA) and the zeta potentials were measured on a Zeta PALS analyzer (Brookhaven Instruments Co.). Photothermal conversion was investigated on a homemade setup as described previously [43].

2.2. Cell culture

2.2.1. Cellular toxicity assay

The RAW 264.7 macrophages and hepatic stellate cells (HSCs) were obtained from Animal Center of Sun Yat-Sen University, China. These cells were cultured on a 96-well plate (1×10^4 cells/well) in Dulbecco's Modified Eagle medium (Gibco BRL) supplemented with 10% (v/v) fetal bovine serum, 100 UI/mL penicillin, and 100 UI/mL streptomycin. The cells were incubated in a humid chamber containing 5% CO_2 at 37 °C. After 12 h, the medium was replaced with 200 μL DMEM medium containing 100 pM/well of the BSA-coated sAuNRs or BSA-coated bAuNRs. The molar concentrations of the AuNRs were calculated based on the method reported previously [44]. The concentration of gold was determined by ICP-OES and the bAuNRs and sAuNRs were considered as cylinders with average dimensions of 56 nm × 14 nm and 30 nm × 7 nm, respectively. Accordingly, the bAuNR and sAuNR quantities were calculated to be 1.5×10^{-16} g and 2.1×10^{-17} g, respectively. Based on the gold atom concentrations and quantity of AuNR, the molar concentrations of AuNRs were determined.

The cells were treated with the samples for 6, 12, 24, and 48 h. MTT (3-(4,5-dimethylthiazol-2-yl)-2,5-diphenyltetrazolium bromide) provided by Sigma Corporation was dissolved in the PBS solution at a concentration of 5 mg/mL and filtered by a 0.22 μM filter to sterilize and remove insoluble residues prior to storage in amber vials at 4 °C. The cell viability was assayed by adding 20 μL of

the MTT PBS solution (5 mg/mL) to each well. After the cells were incubated with MTT at 37 °C for 4 h, the MTT solution was removed and 200 μL of DMSO were added to dissolve the formazan crystals. The absorbance correlated with the number of viable cells in each well was measured on a Thermo Reader at 490 nm. The following formula was used to calculate the inhibition of cell growth: Cell viability (%) = (mean of absolute value of treatment group/mean of absolute value of control) × 100%.

2.2.2. Fluorescence microscopy

Fluorescein isothiocyanate (FITC), a versatile fluorescent agent, was used to label the BSA-coated AuNRs with green fluorescence. In brief, 50 μL of FITC DMSO solution (1 mg/mL) was mixed with 10 mL aqueous solution containing BSA-coated AuNRs (0.3 nM), and the mixture was stirred for 3 h in the dark. The FITC-labeled AuNRs were then separated by centrifugation at 10,000 rpm for 5 min and washed several times with deionized water to remove excess FITC. The RAW264.7 macrophages and HSCs (1×10^4 cells per well) were seeded on 96-well plates and incubated for 15 h. After removing the media, the FITC-labeled BSA-coated bAuNRs and BSA-coated sAuNRs (~100 pM) were added and the cells were cultured for another 3 h in the serum-free medium. Afterwards, the media were removed and the cells were washed twice with cold PBS and incubated with 4′,6-diamidino-2-phenylindole (DAPI) stained for 5 min at a concentration of 0.1 μg/mL. The cells were examined under an Olympus fluorescence microscope with a 40× objective.

2.2.3. ICP-OES measurements for cell uptake of AuNRs

1×10^6 RAW264.7 cells and 1×10^6 HSC cells were incubated with 200 μg of the BSA-coated sAuNRs or BSA-coated bAuNRs for 12 h, respectively and then the cells were carefully washed with PBS buffer three times to remove the unloaded AuNRs. Afterwards, 1×10^6 cells of each kind were trypsinized, counted by the trypan blue exclusion method, soaked in aqua regia overnight, and heated to about 140 °C to get rid of hydrogen chloride and nitrogen oxides until the solution became colorless and clear [52]. After making up to a volume of 5 mL using an aqueous solution containing 2% nitric acid and 1% hydrogen chloride, the total cellular gold content was determined by an inductively-coupled plasma atomic emission spectroscopy (ICP-OES, 7000DV, PerkinElmer).

2.2.4. In vitro photothermal evaluation

The RAW264.7 macrophages and HSCs were cultured on a 24-well plate containing the DMEM medium supplemented with 10% FBS for 24 h (37 °C and 5% CO_2), incubated with the BSA-coated sAuNRs or BSA-coated bAuNRs 100 pM/well for another 12 h, and washed with PBS (10 mM, pH 7.4) and fresh medium. The cells were illuminated by an 808 nm laser (1.0 W/cm^2) for 5 min. The cells were collected afterwards, evaluated for apoptosis or necrosis using Annexin-V/PI double staining in darkness for 10 min at room temperature, and studied by BD FACSAria™ flow cytometry (Becton Dickinson, San Jose, CA, USA).

2.3. In vivo experiments

2.3.1. Synthesis of sAuNRs-laden-macrophages

The RAW264.7 macrophages were infected with lentiviral that carried the GFP reporter gene to show green fluorescence. The macrophages were incubated with lentiviral particles at a ratio of 30 particles to 1 cell in the presence of 10 μg/mL hexadimethrine bromide to improve transduction efficiency. After incubation for 24 h, the cells were harvested and seeded at 1×10^5 cells/mL on the 24-well PSt culture plate with the medium containing 100 pM BSA-coated sAuNRs for 12 h. The sAuNRs-laden-macrophages were harvested, washed with cold PBS, and re-plated for later use. The total cellular Au content was determined by the ICP-OES.

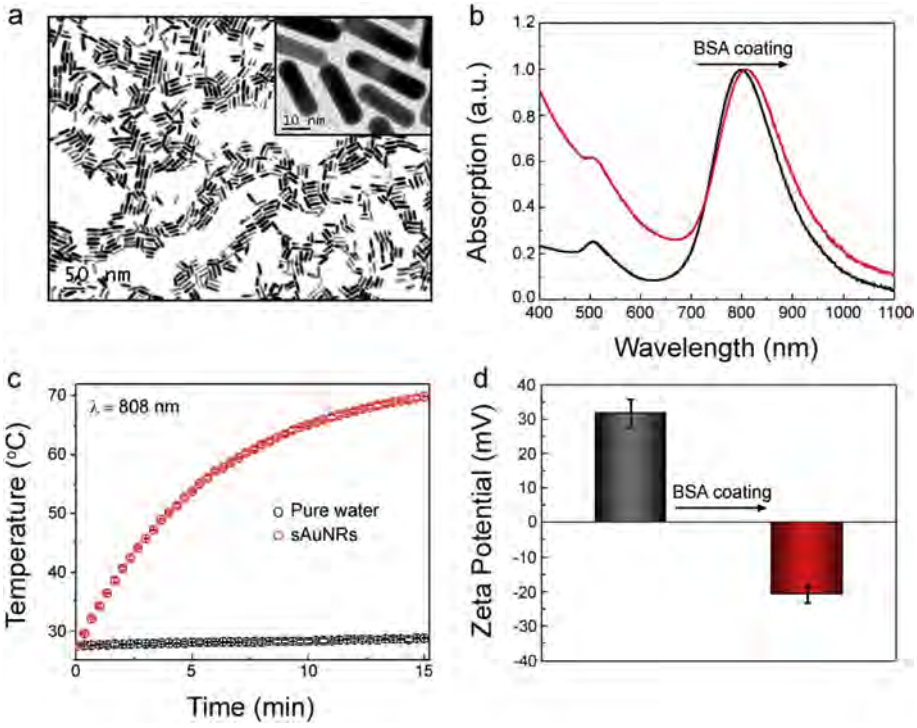

Fig. 1. (a) TEM images of sAuNRs. (b) Normalized absorption spectra of sAuNRs with (red line) and without (black line) the BSA coating. (c) Temperature increase in the sAuNRs solution and pure water under irradiation by an 808 nm laser. (d) Zeta potentials of sAuNRs with and without BSA conjugation. (For interpretation of the references to color in this figure legend, the reader is referred to the web version of this article.)

2.3.2. Macrophage-mediated delivery

Two HepG2 tumor-bearing nude mice were injected intratumorally with either sAuNRs-laden-macrophages (105 μg Au in ~1 × 10^6 macrophages) dispersed in 50 μL of PBS or FITC-labeled sAuNRs (105 μg Au) dispersed in 50 μL of PBS. The *in vivo* biodistributions in the tumors were determined on an *ex/in vivo* fluorescence imaging system (Maestro, USA). After 72 h, the mice were sacrificed and the tumors were extracted immediately for imaging by the same system.

2.3.3. In vivo photothermal treatment

1 × 10^7 HepG2 cells in 100 μL PBS were subcutaneously injected into the left flank of the mice. After one week when the tumors had reached up to ~200 mm^3, the mice were randomly divided into three treatment groups (n = 5 per group). Each group received intratumoral injection of 50 μL of PBS (control), free sAuNRs (105 μg Au) dispersed in 50 μL of PBS, or sAuNRs laden macrophages (105 μg Au in ~1 × 10^6 RAW264.7 macrophages) dispersed in 50 μL of PBS. After 48 h post-injection, the mice were anesthetized by injecting sodium pentobarbital and the entire tumors were exposed to the 808 nm laser (1.0 W/cm^2) for 10 min. The local maximum temperature and infrared thermographic maps were obtained on an infrared thermal imaging camera (Ti27, Fluke, USA). The size of the tumors was measured every two days after the treatment and no mice died during the course of therapy.

2.3.4. Statistical analysis

The results were presented as means or means ± standard deviations (SD) (number of experiments). All the experiments were performed at least in triplicates. The one-way analysis of variance (ANOVA) was adopted to evaluate the significance among the various groups according to the Bonferroni's post-test and a p value of less than 0.05 was considered to be significant.

3. Results and discussion

3.1. Synthesis and characterization

AuNRs are generally synthesized by a seed-mediated method containing two-steps [53,54], but a one-pot seedless method is developed here to synthesize sAuNRs with a smaller diameter of ~7 nm. In this method, nucleation and growth occur in the same solution. NaOL, the sodium salt of a long-chain unsaturated fatty acid, is used to form the CTAB-NaOL which reduces $HAuCl_4$ sufficiently in the presence of ascorbic acid because of its reducing ability of double bonds in molecules. $NaBH_4$ is used as a strong reducing agent in the absence of the seed to enhance the reduction of $Au^+ \rightarrow Au^0$.

Fig. 1a shows the sAuNRs synthesized by the one-pot seedless method. A high yield of sAuNRs with few byproducts can be observed from the TEM image revealing several hundred rods with good dispersibility. The sAuNRs have typical dimensions of (30 ± 5 nm) × (7 ± 1 nm) for an aspect ratio of ~4.1. The LSPR band peaks at about 800 nm as shown in Fig. 1b. The results suggest an efficient technique to prepare sAuNRs with a high yield and good dispersibility.

The photothermal conversion ability of the sAuNRs is illustrated in Fig. 1c. After irradiation with an 808 nm NIR light for 15 min, the temperature of the sAuNRs in the solution increases by about 42.5 °C, whereas that of pure water only increases by about 1.3 °C, indicating that the sAuNRs can rapidly and efficiently convert NIR light into thermal energy. Furthermore, by means of a previously reported method [55], the photothermal conversion efficiency of sAuNRs is ~21%, which is the same as that reported from 14 nm diameter bAuNRs [43].

To facilitate bioconjugation and improve the biocompatibility, the AuNRs are conjugated with BSA using a previously described method [51,56,57]. Fig. 2b shows that BSA modification results in a small red-shift and broadening of the LSPR peak as shown in Fig. 1b. The zeta potential of the sAuNRs changes from +30 to −22 mV (see Fig. 1d) indicative of successful conjugation of BSA to the nanorod surface. The BSA-coated sAuNRs are used in the subsequent *in vitro* and *in vivo* studies.

To compare the size effect on the performance of AuNRs in the subsequent cytotoxicity and cell uptake studies, 14 nm diameter bAuNRs are also synthesized by the common seed-mediated method as the control. As shown in Fig. S1 in Supporting Information, the bAuNRs have dimensions of (56 ± 8 nm) × (14 ± 2 nm) which are bigger than the sAuNRs by a factor of 2, albeit having an almost same aspect ratio (~4.0), LSPR peak wavelength (~800 nm), and photothermal conversion efficiency (21%) after undergoing the same surface modification (BSA conjugation).

3.2. Cytotoxicity investigation

Nanomaterials in cell delivery must have sufficient biocompatibility to ensure that the innate functions of the cells are not

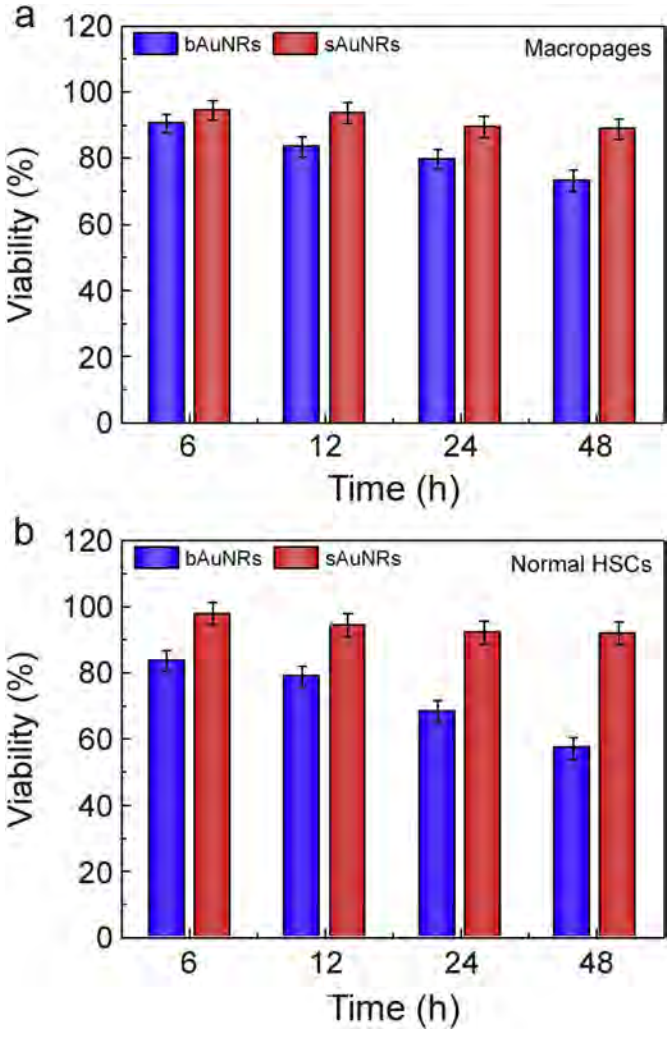

Fig. 2. Cell viability of (a) macrophages and (b) normal HSCs after incubated with 100 pM/well of the BSA-coated sAuNRs or BSA-coated bAuNRs for 6, 12, 24, and 48 h.

impaired or disrupted. Here, the time-dependent cell viability of the BSA-coated sAuNRs for RAW 264.7 macrophages and normal HSCs is examined with the BSA-coated bAuNRs serving as the control sample. As shown in Fig. 2, the smaller sAuNRs exhibit much higher cell viability than bAuNRs. For example, after incubation for 48 h, the cell viability of sAuNRs is as high as (89 ± 3)% for macrophages whereas that of bAuNRs is (73 ± 3)%. With regard to normal HSCs, the cell viability of the sAuNRs is (92 ± 4)% in contrast to (57 ± 3)% for the bAuNRs. It indicates that reduction of the nanorod diameter from 14 to 7 nm decreases the cytotoxicity of the AuNRs rendering them more suitable in clinical applications.

3.3. Cellular uptake

Development of a cell-nanoparticle system with high nanoparticle uptake is essential to photothermal conversion. Herein, the cellular uptake of the BSA-coated sAuNRs and BSA-coated bAuNRs is evaluated by real-time fluorescence microscopy as shown in Fig. 3. In the direct observation, FITC, a versatile fluorescent agent, is used to label the BSA-coated AuNRs with green fluorescence. The emission spectra ($\lambda_{ex} = 490$ nm) of the BSA-coated AuNRs after FITC labeling with different concentrations are shown in Fig. S2. It can be observed that the fluorescence intensity of the FITC is proportional to the concentration of the AuNRs. In contrast, the bare AuNRs (without BSA coating) after FITC labeling show no FITC fluorescence (see Fig. S2). Although AuNRs are well-known fluorescence quenchers, the results demonstrate that attachment of FITC through the BSA spacer produces obvious fluorescence.

The RAW264.7 macrophages are separately incubated with FITC-labeled sAuNRs and FITC-labeled bAuNRs for 6 h and studied by fluorescence microscopy. Panels 1, 2, and 3 in Fig. 3 show the FITC, DAPI, and merged fluorescence images of the macrophages, respectively. The macrophages incubated with the FITC-labeled sAuNRs exhibit green fluorescence throughout the cells and a substantial portion of the intracellular fluorescence is observed from the cytoplasm and nucleus, implying that a substantial amount of the sAuNRs has entered the cells. In contrast, the cells treated with the FITC-labeled bAuNRs show much smaller fluorescence from the local cytoplasm. The results demonstrate higher cell uptake by the sAuNRs for the macrophages than bAuNRs and for normal HSCs, higher cell uptake of sAuNRs can also be observed in comparison with bAuNRs.

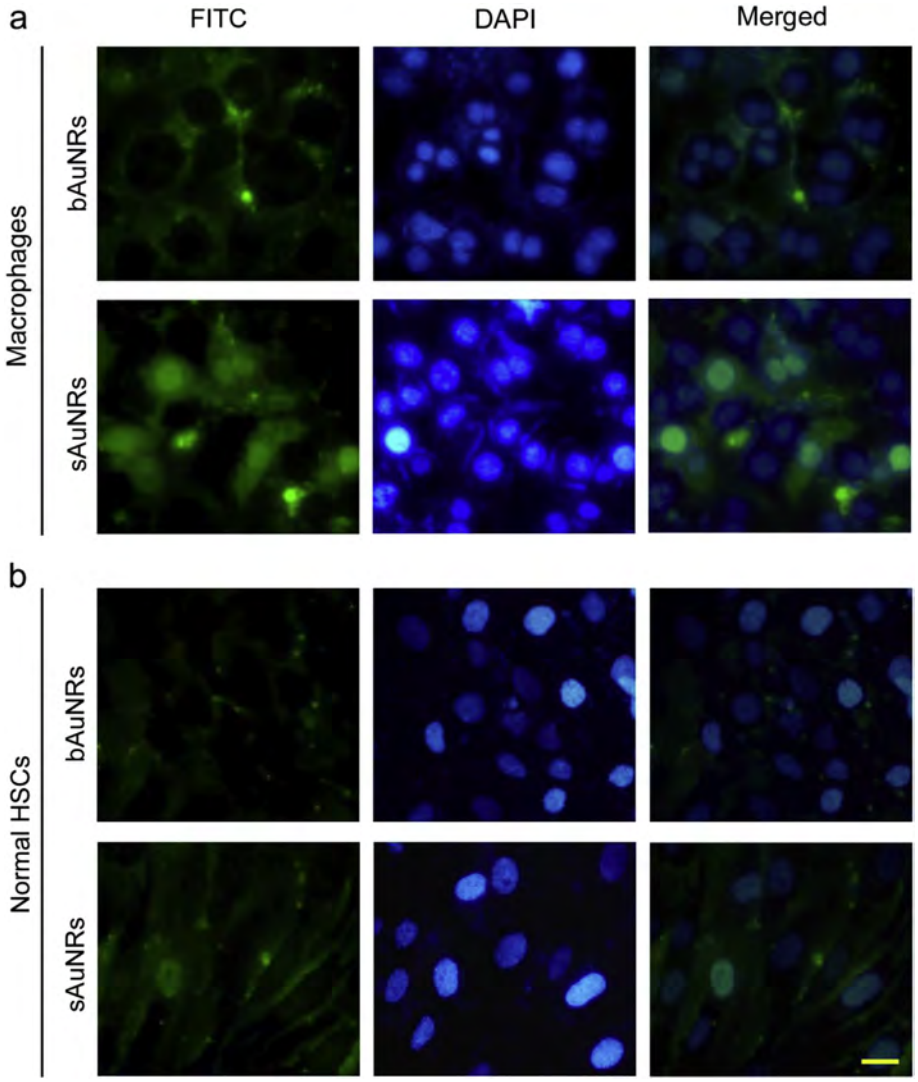

Fig. 3. Fluorescence images of (a) RAW264.7 macrophages and (b) normal HSCs incubated with the BSA-coated sAuNRs and BSA-coated bAuNRs for 6 h. All the AuNRs were labeled with FITC. The cell nuclei are stained with DAPI (blue) and the scale bar is 20 μm. (For interpretation of the references to color in this figure legend, the reader is referred to the web version of this article.)

It is noted that green fluorescence from the FITC-labeled sAuNRs can be observed from some nuclei of the macrophages (see Fig. 3a). In general, localization of Au nanoparticles in the nuclei depends on the particle size, shape, and surface modification [58]. Since the nucleus pore complex in most of the cells is about 39 nm [59], nucleus entry is possible for the Au nanoparticles with a small size [60]. However, according to the fluorescence images, it is difficult to identify whether the sAuNRs are inside or outside the nuclei but nonetheless, Figs. 2 and 3 clearly show the low cytotoxicity and high cell uptake of sAuNRs to the macrophages.

The cell uptake of AuNRs is further analyzed quantitatively (see Fig. 4). 1×10^6 RAW264.7 macrophages were incubated with 200 μg of the BSA-coated sAuNRs or BSA-coated bAuNRs for 12 h and the Au contents in the cells are determined by an ICP-OES. The Au content is 71 μg/1×10^6 cells for the bAuNRs, whereas that of the sAuNRs increases to 105 μg/1×10^6 cells. The results are consistent with fluorescence microscopy observation mentioned above, confirming that the sAuNRs with a smaller size provide higher cell uptake than the bAuNRs. The cell viability and uptake results demonstrate that the sAuNRs have higher cell uptake and lower cytotoxicity simultaneously and are much more biocompatible than the bAuNRs.

Macrophages with the innate phagocytotic capability are recognized to have better uptake ability to nanoparticles than normal cells. A proof-of-principle examination is performed to determine whether the macrophages have better uptake to AuNRs than normal HSCs. The uptake percentage is calculated according to the cellular Au content shown in Fig. 4. The gold content in the macrophages is 105 μg/1×10^6 cells and that in the HSC cells is 45 μg/1×10^6 cells. These values are divided by 200 μg/1×10^6 (the original amount of the BSA-coated sAuNRs) to demonstrate that the macrophages have 52.5% uptake of the sAuNRs and HSCs only have 22.5%. The results agree with the fluorescence images in Fig. 3. A similar difference between the macrophages and HSCs can also be observed from bAuNRs. The macrophages show 35.3% uptake of bAuNRs but the HSCs only show 14.0%. The RAW264.7 macrophages are derived from myeloid progenitor cells in the bone marrow. As implied by the name (big eaters, from makros “large” phagein “eat”), the primary functions of the macrophages are to engulf foreign materials and digest them in the body [25]. Here, the sAuNRs with high cell uptake and low cytotoxicity to macrophages enable the establishment of the efficient macrophage-mediated delivery system.

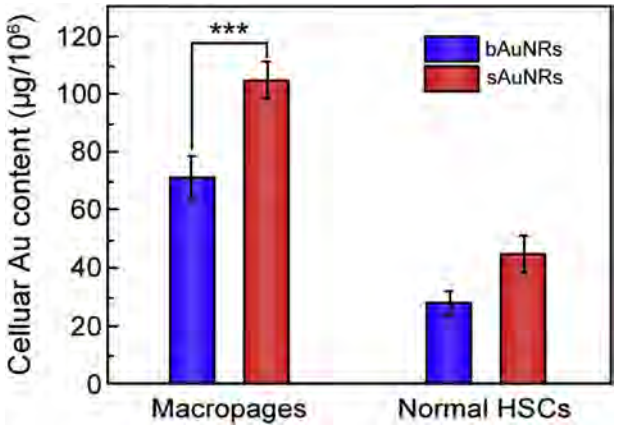

Fig. 4. Celluar uptake of BSA-coated bAuNRs and BSA-coated sAuNRs to RAW264.7 macrophages and normal HSCs.

3.4. Photothermal effect of sAuNRs endocytosed by macrophages

The photothermal effect of the sAuNRs endocytosed by macrophages is examined (see Fig. 5). The RAW264.7 macrophages are incubated with sAuNRs and bAuNRs for 12 h and the cells are illuminated with the 808 nm NIR laser for 10 min. The cells are collected after irradiation and detected for apoptosis or necrosis using Annexin-V/PI double staining. The cells incubated with AuNRs show significant cell death, whereas the AuNRs-free cells show a viability of more than 97% after laser irradiation (Fig. 5a), indicating that the AuNRs endocytosed by macrophages retain the powerful photothermal conversion ability. Furthermore, the sAuNRs induce a larger cell apoptosis ratio of (32.6 ± 0.87)% (Fig. 5c) in comparison with the bAuNRs of only (17.9 ± 1.08)% (Fig. 5b). Considering that the two AuNRs have almost the same photothermal conversion efficiency, the higher PTT effects of sAuNRs in macrophages is probably due to the larger uptake dose. The results suggest that macrophages loaded with sAuNRs deliver higher photothermal performance than those loaded with bigger bAuNRs.

3.5. In vivo delivery and PTT studies

According to the above results, smaller sAuNRs have higher cell viability for the macrophages than bAuNRs. The cell viability of sAuNRs is as high as (89 ± 3)% for macrophages whereas that of bAuNRs is only (73 ± 3)%. Furthermore, the macrophages show 52.5% uptake of sAuNRs but it is only 35.8% for the bAuNRs. Correspondingly, the macrophages loaded with sAuNRs deliver better photothermal performance than those loaded with bAuNRs. These results demonstrate that sAuNRs are more suitable for cell-mediated delivery and photothermal therapy and consequently, the macrophages loaded with sAuNRs (named sAuNRs-laden-macrophages) are employed in subsequent *in vivo* studies.

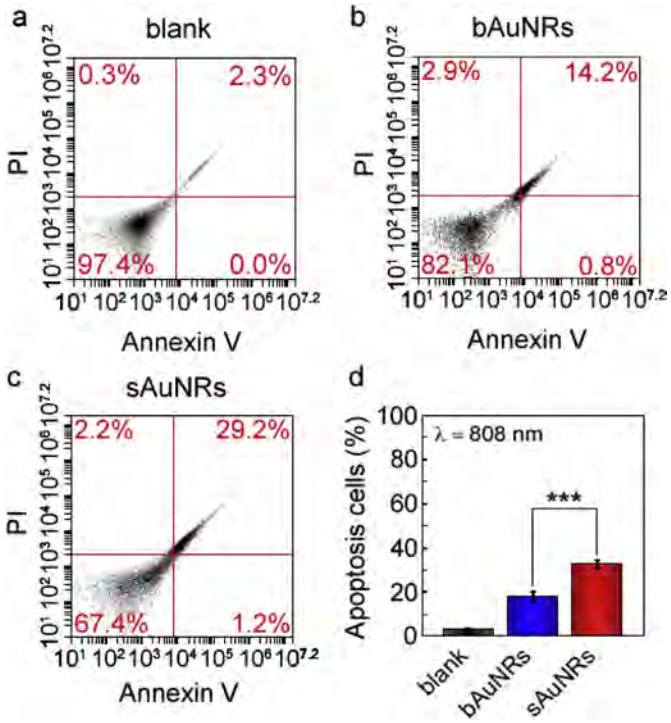

Fig. 5. (a–c) Flow cytometry analysis of the PTT effects of BSA-coated sAuNRs and BSA-coated bAuNRs on apoptosis of macrophages with an 808 nm NIR laser irradiation for 10 min. (d) Statistical results showing the percentage of apoptosis in macrophages after different treatments.

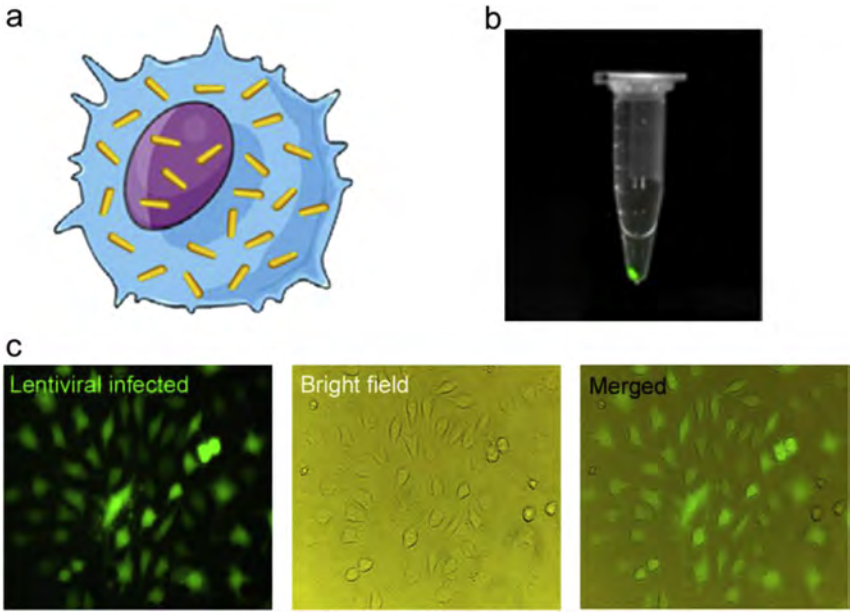

Fig. 6. (a) Diagram of sAuNRs-laden-macrophages. (b) Fluorescence image of solution containing sAuNRs-laden-macrophages in the bottom. (c) Fluorescence, bright field, and merged images of sAuNRs-laden-macrophages. The macrophages are infected with lentiviral carrying the GFP reporter gene with green fluorescence. (For interpretation of the references to color in this figure legend, the reader is referred to the web version of this article.)

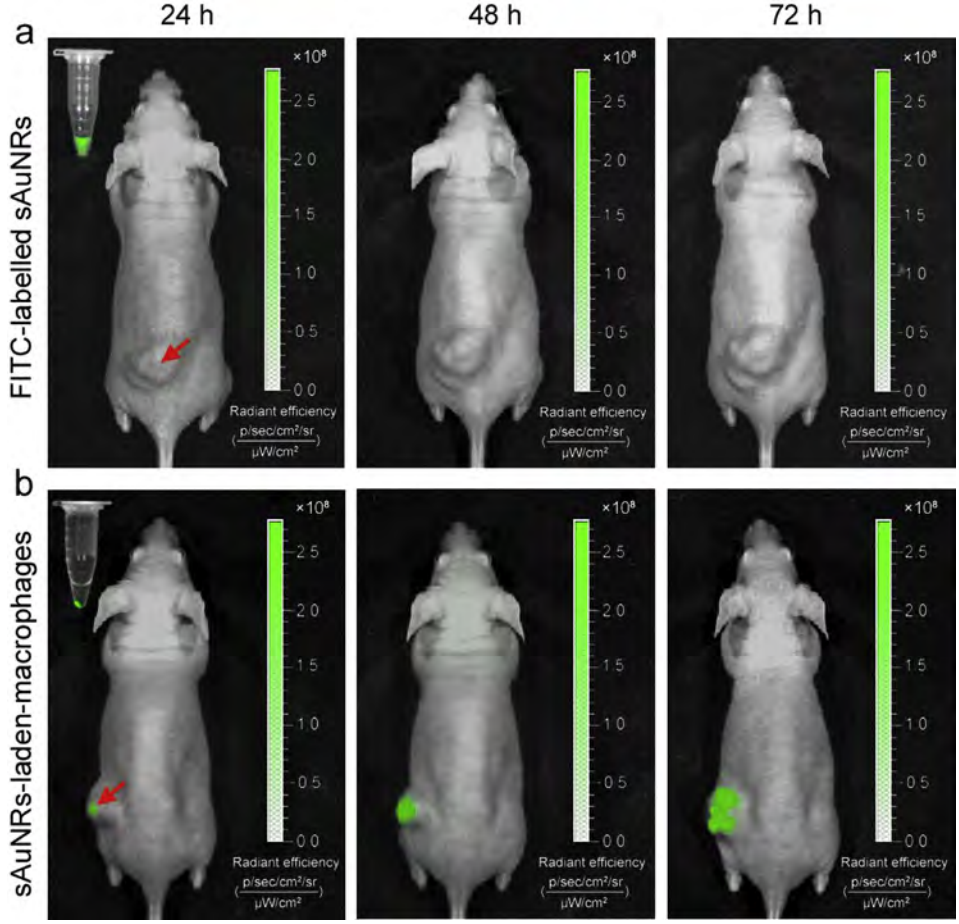

Fig. 7. *In vivo* fluorescence images of intratumoral distribution 24, 48, and 72 h after intratumoral injection with (a) FITC-labeled sAuNRs and (b) sAuNRs-laden-macrophages. Insets: Fluorescence images of the solution containing the samples.

The RAW264.7 macrophages are first infected with lentiviral that carries the GFP reporter gene to show green fluorescence, then incubated with the sAuNRs for 12 h. As shown in Fig. 6, the sAuNRs-laden-macrophages (containing 105 μg Au/10^6 cells) exhibit green fluorescence and unaltered cell morphology. A distribution study is performed to determine whether the macrophage loading alters the intratumoral distribution of the sAuNRs (see Fig. 7). Two HepG2 tumor-bearing nude mice are injected intratumorally with either the sAuNRs-laden-macrophages (105 μg Au in ~1 × 10^6 macrophages) or FITC-labeled sAuNRs suspensions (105 μg Au). The injection site is near the central core of the tumor. The *in vivo* biodistributions in the tumors are observed on an *ex*/*in vivo* fluorescence imaging system.

As shown in Fig. 7a and Fig. S3, no fluorescence is observed from the mice tumor even after 72 h intratumoral injection of the FITC-labeled sAuNRs. This suggests that the AuNRs distribution is localized in the central core of the tumor after injection and green fluorescence with poor tissue penetration cannot be traced. The results are in line with the common view that the injected nanoparticles are unable to penetrate the tumor mass. In contrast, strong green fluorescence is observed from the tumor injected with the sAuNRs-laden-macrophages (Fig. 7b and Fig. S3), indicating that a large number of sAuNRs-laden-macrophages can infiltrate the tumor even reaching the tumor border. These results demonstrate the greatly enhanced tumor coverage of the sAuNRs *via* the macrophage vehicles. Hypoxic tumor cells can secret various chemoattractants such as vascular endothelial growth factors in the tumor microenvironment to enhance the penetration ability of the macrophages into tumors [61]. The tumor associated macrophage can even constitute up to 80% of the tumor mass [26] and therefore, the use of macrophages to facilitate sAuNRs delivery can overcome the extracelluar matrix and penetrate more deeply into the tumor resulting in enhanced tumor coverage.

The *in vivo* therapeutic efficacy of the sAuNRs-laden-macrophages is further evaluated using HepG2 tumor-bearing nude mice (see Fig. 8). When the tumor reaches approximately 200 mm^3, the mice are randomly divided into four groups and intratumorally injected with PBS, free macrophages, free sAuNR suspensions, and sAuNRs-laden-macrophages, respectively. NIR light irradiation (1.0 W/cm^2 and 808 nm) is conducted on the tumors 48 h after intratumoral injection. The maximum temperature and infrared thermographic maps are recorded by an infrared thermal imaging camera. The tumor volume in each NIR irradiation group is measured by a caliper every other day to determine the tumor growth and the results are plotted as a function of time. The mice are at day 14 for tumor collection and no mice die during the course of therapy.

As shown in Fig. 8a and b, under the 808 nm NIR light irradiation, the maximum temperature of the tumor treated with free sAuNRs increases from 34.4 to 38.9 °C during the first 1 min and reaches 43.6 °C after 10 min. In contrast, the maximum temperature of the tumor treated with the sAuNRs-laden-macrophages increases from 34.5 to 44.3 °C during the first 1 min and reaches as high as 53.8 °C after 10 min. It is known that a temperature over 43 °C can destroy cancer cells due to the lower heat tolerance caused by poor blood supply [62]. The thermal imaging maps in

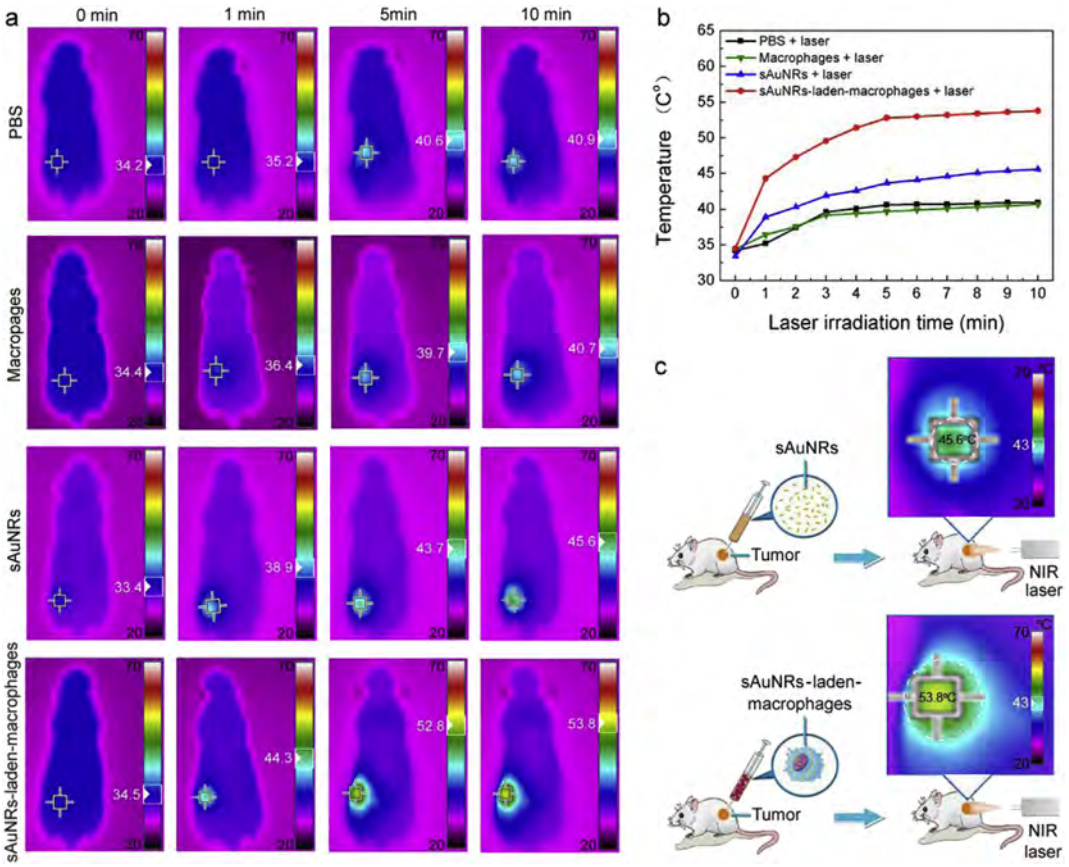

Fig. 8. (a) Infrared thermal images and (b) Time-dependent temperature increase of HepG2 tumor-bearing nude mice under an 808 nm light irradiation 48 h post intratumoral injection of PBS, free macrophages, free BSA-coated sAuNRs (105 μg Au), and BSA-coated sAuNRs-laden-macrophages (105 μg Au in ~1 × 10^6 macrophages). The color bar refers to the relative temperature values. (c) Diagram highlighting the difference between the treatment of free BSA-coated sAuNRs and BSA-coated sAuNRs-laden-macrophages. (For interpretation of the references to color in this figure legend, the reader is referred to the web version of this article.)

Fig. 8c show that the high-temperature area (over 43 °C) in the tumor treated with the sAuNRs-laden-macrophages is obviously larger than that with free sAuNRs. The results are consistent with the aforementioned distribution studies in which the sAuNRs-laden-macrophages show enhanced tumor coverage of the sAuNRs. A single heat source is inefficient for the delivery of thermal energy to a large volume of tissue [63]. Since the sAuNRs after free sAuNRs injection are localized near the injection site of the tumor, most of the thermal energy is wasted on the adjacent necrotic tissues and thermal conduction mainly depends on tissue perfusion. In contrast, the sAuNRs-laden-macrophages with enhanced tumor coverage show an even distribution of heat generation with regard to the sAuNRs thus increasing the temperature almost everywhere in the tumor.

The tumor volume variations are consistent with those of temperature (see Fig. 9). With regard to the tumor treated with free sAuNRs, although the maximum temperature reaches the threshold (over 43 °C) to kill cancer cells, the temperature of some tumor margins is catabatic. Hence, tumor growth is only inhibited in the first 6 days and tumor recurrence is observed afterwards. For the tumors treated with the sAuNRs-laden-macrophages, since the temperature in the entire tumor is high enough to kill the cancer cells, almost 95% tumor inhibition is achieved on the 14th day and no tumor recurrence is observed. The results demonstrate the excellent antitumor efficiency of the sAuNRs-laden-macrophages in comparison with free sAuNRs. As the control groups, the PBS and free macrophages result in only about 6 °C increase in the maximum temperature of the tumor and it is far from sufficient to kill cancer cells. As a result, the tumors grew progressively with the tumor volume increasing from 200 mm^3 to approximately 1600 mm^3 after 14 days.

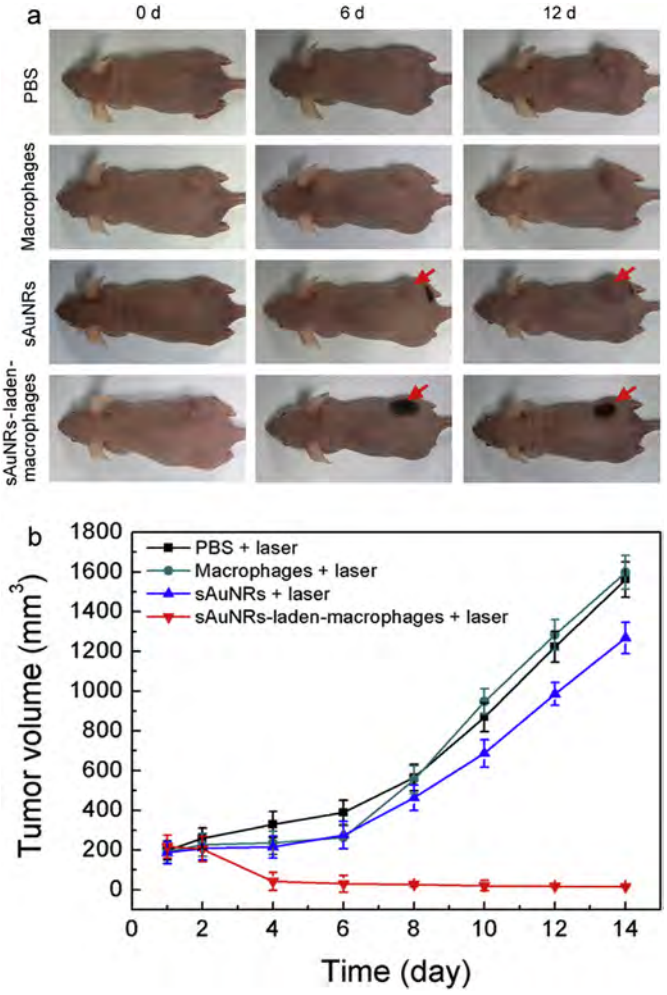

Fig. 9. Photothermal ablation of tumors in the mice by intratumorally injected with PBS, free macrophages, free BSA-coated sAuNRs (105 μg Au) and BSA-coated sAuNRs-laden-macrophages (10^5 μg Au in ~1 × 10^6 macrophages). (a) Typical photographs of the mice after the treatments for 0, 6, and 12 days and (b) Growth of tumors in the different groups of mice after the treatments.

It is known that nanomaterials-mediated photothermal cancer therapy is a potentially curative treatment modality that is undergoing rapid recent technological advancements. Currently, one of the greatest challenges of translating PTT into clinical use is how to optimize the *in vivo* agent delivery to achieve a homogenous agent distribution within the tumor. In our research, ascribed to the high cell uptake and low cytotoxicity of the sAuNRs to macrophages, the sAuNRs-laden-macrophages are successfully established for the *in vivo* PTT studies. As aforementioned, the use of macrophages to facilitate sAuNRs delivery can overcome the extracelluar matrix and penetrate more deeply into the tumor resulting in enhanced tumor coverage. The sAuNRs-laden-macrophages under NIR light irradiation show an even distribution of heat generation resulting in minimized tumor recurrence rates. These results suggest a desirable approach to improve the PTT efficiency by optimizing the intratumoral distribution of the agents. Furthermore, the macrophages themselves can be engineered to carry imaging agents such as GFP lentiviral to combine treatment and imaging strategies for cancer diagnostics and therapy.

4. Conclusion

In conclusion, an efficient delivery and photothermal ablation system with sAuNRs-laden-macrophages is described for cancer therapy. The system is established by using macrophages as Trojan horses carrying 7 nm diameter sAuNRs which have higher cell uptake and lower cytotoxicity than the commonly used 14 nm diameter bAuNRs. With the greatly enhanced tumor coverage, the sAuNRs-laden-macrophages exhibit improved photothermal conversion everywhere in the tumor and the tumor recurrence rate is greatly reduced in comparison with free sAuNRs. The findings suggest an efficient PTT approach by optimizing *in vivo* agent delivery. Furthermore, this cell-mediated delivery can also be extended to other nanoparticles or drugs-based therapeutics. These findings highlight the advantages of combining cellular therapies and nanotechnology to contrive more effective cancer treatments.

Acknowledgments

The authors acknowledge financial support from the National Natural Science Foundations of China (51372175, 81501592), Science and Technology Key Project of Shenzhen (JCYJ20140417113430608), Shenzhen Key Laboratory for Molecular Biology of Neural Development (ZDSY20120617112838879), Hong Kong Research Grants Council (RGC) General Research Funds (GRF) No, CityU 112212, and City University of Hong Kong Strategic Research Grant (SRG) No. 7004188.

Appendix A. Supplementary data

Supplementary data related to this article can be found at http://dx.doi.org/10.1016/j.biomaterials.2015.09.038.

References

[1] L. Cheng, C. Wang, L. Feng, K. Yang, Z. Liu, Functional nanomaterials for

phototherapies of cancer, Chem. Rev. 114 (2014) 10869–10939.
[2] L.R. Hirsch, R.J. Stafford, J.A. Bankson, S.R. Sershen, B. Rivera, R.E. Price, et al., Nanoshell-mediated near-infrared thermal therapy of tumors under magnetic resonance guidance, Proc. Natl. Acad. Sci. U. S. A. 11 (2003) 13549–13554.
[3] D.P. O'Neal, L.R. Hirsch, N.J. Halas, J.D. Payne, J.L. West, Photo-thermal tumor ablation in mice using near infrared-absorbing nanoparticles, Cancer Lett. 209 (2004) 171–176.
[4] P.K. Jain, I.H. El-Sayed, M.A. El-Sayed, Au nanoparticles target cancer, Nano Today 2 (2007) 18–29.
[5] G. Von Maltzahn, J.H. Park, A. Agrawal, N.K. Bandaru, S.K. Das, M.J. Sailor, et al., Computationally guided photothermal tumor therapy using long-circulating gold nanorod antennas, Cancer Res. 69 (2009) 3892–3900.
[6] X.H. Huang, I.H. El-Sayed, W. Qian, M.A. El-Sayed, Cancer cell imaging and photothermal therapy in the near-infrared region by using gold nanorods, J. Am. Chem. Soc. 128 (2006) 2115–2120.
[7] T.S. Hauck, T.L. Jennings, T. Yatsenko, J.C. Kumaradas, W.C.W. Chan, Enhancing the toxicity of cancer chemotherapeutics with gold nanorod hyperthermia, Adv. Mater. 20 (2008) 3832–3838.
[8] D. Ni, H. Ding, S. Liu, H. Yue, Y. Bao, Z. Wang, et al., Drug delivery: superior intratumoral penetration of paclitaxel nanodots strengthens tumor restriction and metastasis prevention, Small 11 (2015) 2465.
[9] M.S. Yavuz, Y. Cheng, J. Chen, C.M. Cobley, Q. Zhang, M. Rycenga, et al., Gold nanocages covered by smart polymers for controlled release with near-infrared light, Nat. Mater. 8 (2009) 935–939.
[10] J.T. Robinson, S.M. Tabakman, Y. Liang, H. Wang, H. Sanchez Casalongue, D. Vinh, et al., Ultrasmall reduced graphene oxide with high near-infrared absorbance for photothermal therapy, J. Am. Chem. Soc. 133 (2011) 6825–6831.
[11] N.W. Kam, M. O'Connell, J.A. Wisdom, H. Dai, Carbon nanotubes as multifunctional biological transporters and near-infrared agents for selective cancer cell destruction, Proc. Natl. Acad. Sci. U. S. A. 102 (2005) 11600–11605.
[12] C.M. Hessel, V.P. Pattani, M. Rasch, M.G. Panthani, B. Koo, J.W. Tunnell, et al., Copper selenide nanocrystals for photothermal therapy, Nano Lett. 11 (2011) 2560–2566.
[13] B. Yu, M. Yang, L. Shi, Y. Yao, Q. Jiang, X. Li, et al., Explicit hypoxia targeting with tumor suppression by creating an "obligate" anaerobic Salmonella Typhimurium strain, Sci. Rep. 2 (2012) 436.
[14] B. Tian, C. Wang, S. Zhang, L. Feng, Z. Liu, Photothermally enhanced photodynamic therapy delivered by nano-graphene oxide, ACS Nano 5 (2011) 7000–7009.
[15] X. Huang, S. Neretina, M.A. El-Sayed, Gold nanorods: from synthesis and properties to biological and biomedical applications, Adv. Mater. 21 (2009) 4880–4910.
[16] W. Liu, X. Li, Y.S. Wong, W. Zheng, Y. Zhang, W. Cao, et al., Selenium nanoparticles as a carrier of 5-fluorouracil to achieve anticancer synergism, ACS Nano 6 (2012) 6578–6591.
[17] K. Yang, S. Zhang, G. Zhang, X. Sun, S.T. Lee, Z. Liu, Graphene in mice: ultrahigh In vivo tumor uptake and efficient photothermal therapy, Nano Lett. 10 (2010) 3318–3323.
[18] M.A. El-Sayed, Concluding remarks: summary of some of our recent studies in the field of conjugating plasmonic gold nanoparticles to single cancer cells and their molecular and cellular dynamics, Faraday Discuss. 175 (2014) 305–308.
[19] M. Li, X. Yang, J. Ren, K. Qu, X. Qu, Using graphene oxide high near-infrared absorbance for photothermal treatment of Alzheimer's disease, Adv. Mater. 24 (2012) 1722–1728.
[20] B. Li, K. Ye, Y. Zhang, J. Qin, R. Zou, K. Xu, et al., Photothermal theragnosis synergistic therapy based on bimetal sulphide nanocrystals rather than nanocomposites, Adv. Mater. 27 (2015) 1339–1345.
[21] M. Longmire, P.L. Choyke, H. Kobayashi, Clearance properties of nano-sized particles and molecules as imaging agents: considerations and caveats, Nanomedicine 3 (2008) 703–717.
[22] M.A. El-Sayed, A.A. Shabaka, O.A. El-Shabrawy, N.A. Yassin, S.S. Mahmoud, S.M. El-Shenawy, et al., Tissue distribution and efficacy of gold nanorods coupled with laser induced photoplasmonic therapy in ehrlich carcinoma solid tumor model, PLoS One 8 (2013) 1–9.
[23] D.B. Chithrani, M. Dunne, J. Stewart, C. Allen, D.A. Jaffray, Cellular uptake and transport of gold nanoparticles incorporated in a liposomal carrier, Nanomedicine 6 (2010) 161–169.
[24] M.R. Choi, K.J. Stanton-Maxey, J.K. Stanley, C.S. Levin, R. Bardhan, D. Akin, et al., A cellular Trojan Horse for delivery of therapeutic nanoparticles into tumors, Nano Lett. 7 (2007) 3759–3765.
[25] S.J. Madsen, S.K. Baek, A.R. Makkouk, T. Krasieva, H. Hirschberg, Macrophages as cell-based delivery systems for nanoshells in photothermal therapy, Ann. Biomed. Eng. 40 (2012) 507–515.
[26] J. Choi, H.Y. Kim, E.J. Ju, J. Jung, J. Park, H.K. Chung, et al., Use of macrophages to deliver therapeutic and imaging contrast agents to tumors, Biomaterials 33 (2012) 4195–4203.
[27] R. Mooney, L. Roma, D. Zhao, D. Van Haute, E. Garcia, S.U. Kim, et al., Neural stem cell-mediated delivery of gold nanorods improves photothermal therapy, ACS Nano 8 (2014) 12450–12460.
[28] L. Li, Y. Guan, H. Liu, N. Hao, T. Liu, X. Meng, et al., Silica nanorattle-doxorubicin-anchored mesenchymal stem cells for tumor-tropic therapy, ACS Nano 5 (2011) 7462–7470.
[29] M.T. Stephan, S.B. Stephan, P. Bak, J. Chen, D.J. Irvine, Synapse-directed delivery of immunomodulators using T-cell-conjugated nanoparticles, Biomaterials 33 (2012) 5776–5787.
[30] C. Christie, S.J. Madsen, Q. Peng, H. Hirschberg, Macrophages as nanoparticle delivery vectors for photothermal therapy of brain tumors, Ther. Deliv. 6 (2015) 371–384.
[31] X. Huang, F. Zhang, H. Wang, G. Niu, K.Y. Choi, M. Swierczewska, et al., Mesenchymal stem cell-based cell engineering with multifunctional mesoporous silica nanoparticles for tumor delivery, Biomaterials 34 (2013) 1772–1780.
[32] R. Mooney, L. Roma, D. Zhao, D. Van Haute, E. Garcia, S.U. Kim, A.J. Annala, et al., Neural stem cell-mediated intratumoral delivery of gold nanorods improves photothermal therapy, ACS Nano 8 (2014) 12450–12460.
[33] S.K. Patel, J.M. Janjic, Macrophage targeted theranostics as personalized nanomedicine strategies for inflammatory diseases, Theranostics 5 (2015) 150–172.
[34] A.C. Anselmo, S. Mitragotri, Cell-mediated delivery of nanoparticles: taking advantage of circulatory cells to target nanoparticles, J. Control Release 190 (2014) 531–541.
[35] C. Loo, A. Lowery, N. Halas, J. West, R. Drezek, Immunotargeted nanoshells for integrated cancer imaging and therapy, Nano Lett. 5 (2005) 709–711.
[36] C. Loo, L. Hirsch, M.H. Lee, E. Chang, J. West, N. Halas, et al., Gold nanoshell bioconjugates for molecular imaging in living cells, Opt. Lett. 30 (2005) 1012–1014.
[37] X.M. Zhu, C. Fang, H. Jia, Y. Huang, C.H. Cheng, C.H. Ko, et al., Cellular uptake behavior, photothermal therapy performance, and cytotoxicity of gold nanorods with various coatings, Nanoscale 6 (2014) 11462–11472.
[38] E. Yasun, C. Li, I Barut, D. Janvier, L. Qiu, C. Cui, et al., BSA modification to reduce CTAB induced nonspecificity and cytotoxicity of aptamer-conjugated gold nanorods, Nanoscale 7 (2015) 10240–10248.
[39] E.B. Dickerson, E.C. Dreaden, X.H. Huang, I.H. El-Sayed, H. Chu, S. Pushpanketh, et al., Gold nanorod assisted near-infrared plasmonic photothermal therapy (PPTT) of squamous cell carcinoma in mice, Cancer Lett. 269 (2008) 57–66.
[40] L. Wang, Y. Liu, W. Li, X. Jiang, Y. Ji, X. Wu, et al., Selective targeting of gold nanorods at the mitochondria of cancer cells: implications for cancer therapy, Nano Lett. 11 (2011) 772–780.
[41] Y. Xu, J. Wang, X. Li, Y. Liu, L. Dai, X. Wu, et al., Selective inhibition of breast cancer stem cells by gold nanorods mediated plasmonic hyperthermia, Biomaterials 35 (2014) 4667–4677.
[42] W.Q. Li, C.Y. Sun, F. Wang, Y.C. Wang, Y.W. Zhai, M. Liang, et al., Achieving a new controllable male contraception by the photothermal effect of gold nanorods, Nano Lett. 13 (2013) 2477–2484.
[43] B. Wang, J.H. Wang, Q. Liu, H. Huang, M. Chen, K. Li, et al., Rose-bengal-conjugated gold nanorods for *in vivo* photodynamic and photothermal oral cancer therapies, Biomaterials 35 (2014) 1954–1966.
[44] N.G. Khlebtsov, Determination of size and concentration of gold nanoparticles from extinction spectra, Anal. Chem. 80 (2008) 6620–6625.
[45] P.K. Jain, K.S. Lee, I.H. El-Sayed, M.A. El-Sayed, Calculated absorption and scattering properties of gold nanoparticles of different size, shape, and composition: applications in biological imaging and biomedicine, J. Phys. Chem. B 110 (2006) 7238–7248.
[46] X. Huang, I.H. El-Sayed, W. Qian, M.A. El-Sayed, Cancer cell imaging and photothermal therapy in the near-infrared region by using gold nanorods, J. Am. Chem. Soc. 128 (2006) 2115–2120.
[47] H. Klingberg, S. Loft, L.B. Oddershede, P. Møller, The influence of flow, shear stress and adhesion molecule targeting on gold nanoparticle uptake in human endothelial cells, Nanoscale 7 (2015) 11409–11419.
[48] W. Jiang, B.Y. Kim, J.T. Rutka, W.C. Chan, Nanoparticle-mediated cellular response is size-dependent, Nat. Nanotechnol. 3 (2008) 145–150.
[49] T.K. Sau, C.J. Murphy, Seeded high yield synthesis of short Au nanorods in aqueous solution, Langmuir 20 (2004) 6414–6420.
[50] P.S. Isabel, P.J. Jorge, M.L.M. Luis, Silica-coating and hydrophobation of CTAB-stabilized gold nanorods, Chem. Mater. 18 (2006) 2465–2467.
[51] M.R. Ali, S.R. Panikkanvalappil, M.A. El-Sayed, Enhancing the efficiency of gold nanoparticles treatment of cancer by increasing their rate of endocytosis and cell accumulation using rifampicin, J. Am. Chem. Soc. 136 (2014) 4464–4467.
[52] Y. Qiu, Y. Liu, L. Wang, L. Xu, R. Bai, Y. Ji, et al., Surface chemistry and aspect ratio mediated cellular uptake of Au nanorods, Biomaterials 31 (2010) 7606–7619.
[53] T.K. Sau, C.J. Murphy, Seeded high yield synthesis of short Au nanorods in aqueous solution, Langmuir 20 (2004) 6414–6420.
[54] J.H. Wang, B. Wang, Q. Liu, Q. Li, H. Huang, L. Song, et al., Bimodal optical diagnostics of oral cancer based on rose bengal conjugated gold nanorod platform, Biomaterials 34 (2013) 4274–4283.
[55] D.K. Roper, W. Ahn, M. Hoepfner, Microscale heat transfer transduced by surface plasmon resonant gold nanoparticles, J. Phys. Chem. C 111 (2007) 3636–3641.
[56] K.M. Au, S.P. Armes, Heterocoagulation as a facile route to prepare stable serum albumin-nanoparticle conjugates for biomedical applications: synthetic protocols and mechanistic insights, ACS Nano 6 (2012) 8261–8279.
[57] P. Khullar, V. Singh, A. Mahal, P.N. Dave, S. Thakur, G. Kaur, et al., Bovine serum albumin bioconjugated gold nanoparticles: synthesis, hemolysis, and cytotoxicity toward cancer cell lines, J. Phys. Chem. C 116 (2012) 8834.
[58] K.M. Au, S.P. Armes, Heterocoagulation as a facile route to prepare stable serum albumin-nanoparticle conjugates for biomedical applications: synthetic protocols and mechanistic insights, ACS Nano 6 (2012) 8261–8279.

[59] Y.J. Gu, J. Cheng, C.C. Lin, Y.W. Lam, S.H. Cheng, W.T. Wong, Nuclear penetration of surface functionalized gold nanoparticles, Toxicol. Appl. Pharmacol. 237 (2009) 196–204.
[60] X. Cheng, X. Tian, A. Wu, J. Li, Y. Chong, Z. Chai, et al., Protein corona influences cellular uptake of gold nanoparticles by phagocytic and nonphagocytic cells in a size-dependent manner, ACS Appl. Mater. Interfaces 7 (2015) 20568–20575.
[61] A. Eljazewicz, M. Wiese, A. Melmin-Basa, M. Jankowski, L. Gackowska, I. Kubiszewska, et al., Collaborating with the enemy: function of macrophages in the development of neoplastic disease, Mediat. Inflamm. 2013 (2013) 1–11.
[62] X. Cheng, X. Tian, A. Wu, J. Li, Y. Chong, Z. Chai, et al., Protein corona influences cellular uptake of gold nanoparticles by phagocytic andnonphagocytic cells in a size-dependent manner, ACS Appl. Mater. Interfaces 7 (2015) 20568–20575.
[63] D.K. Roper, W. Ahn, M. Hoepfner, Microscale heat transfer transduced by surface plasmon resonant gold nanoparticles, J. Phys. Chem. C 111 (2007) 3636–3641.

Supporting Information for

Small Gold Nanorods Laden Macrophages for Enhanced Tumor Coverage in Photothermal Therapy

Zhibin Li[a], Hao Huang[a], Siying Tang[a], Yong Li[a], Xue-Feng Yu[a]*, Huaiyu Wang[a,b], Penghui Li[a,b], Zhengbo Sun[a,c], Han Zhang[c], Chenli Liu[a], Paul K Chu[b]*

[a] *Institute of Biomedicine and Biotechnology, Shenzhen Institutes of Advanced Technology, Chinese Academy of Sciences, Shenzhen 518055, Guangdong, P. R. China*

[b] *Department of Physics and Materials Science, City University of Hong Kong, Tat Chee Avenue, Kowloon, Hong Kong*

[c] *SZU-NUS Collaborative Innovation Center for Optoelectronic Science and Technology, Key Laboratory of Optoelectronic Devices and Systems of Ministry of Education and Guangdong Province, College of Optoelectronic Engineering, Shenzhen University, Shenzhen 518060, Guangdong, P. R. China*

*Corresponding authors: Tel: +852-34427724; Fax: +852-34420538 (P.K. Chu)

E-mail addresses: yxf@whu.edu.cn (X.-F. Yu); paul.chu@cityu.edu.hk (P. K. Chu)

Keywords: photothermal therapy; gold nanorods; macrophages; nanoparticle delivery; tumors.

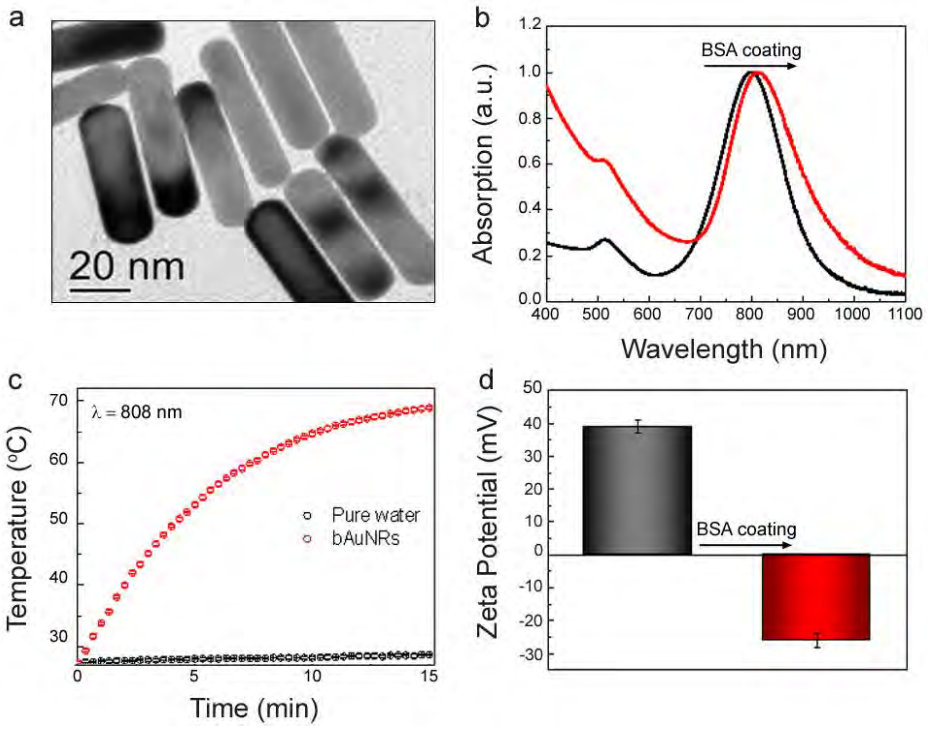

Fig. S1. (a) TEM image of bAuNRs. (b) Normalized absorption spectra of bAuNRs with (red line) and without (black line) the BSA coating. (c) Temperature increase observed from bAuNRs under an 808 nm light irradiation. (d) Zeta potentials of bAuNRs with and without BSA conjugation.

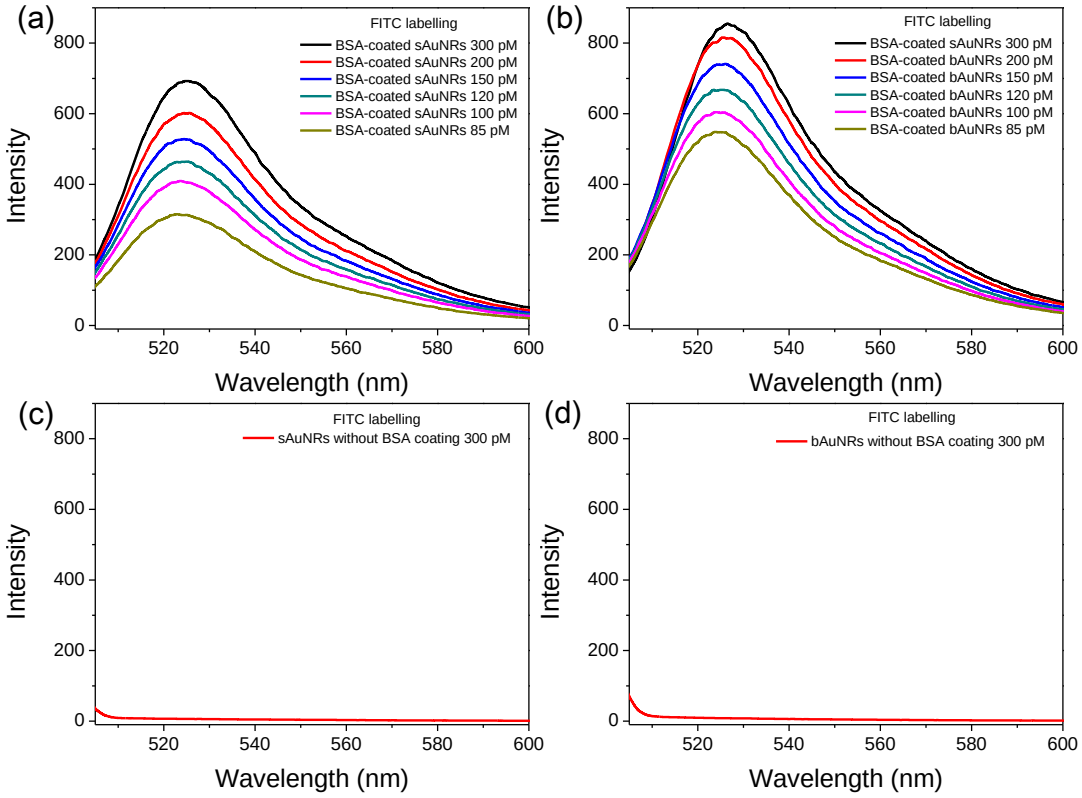

Fig. S2. (a, b) Emission spectra (λ_{ex} = 490 nm) of (a) BSA-coated sAuNRs and (b) BSA-coated bAuNRs with different concentrations from 85 to 300 pM. (c, d) Emission spectra (λ_{ex} = 490 nm) of (c) sAuNRs and (b) bAuNRs with concentrations of 300 pM. All the AuNRs are labeled with FITC.

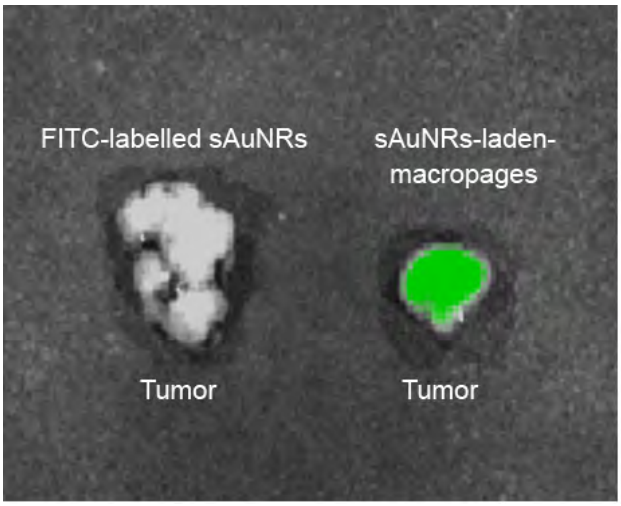

Fig. S3. Intratumoral distributions of FITC-labelled sAuNRs and sAuNRs-laden-macropages. On day 3 after intratumoral injection of the samples, the mice are sacrificed and the tumors are extracted for imaging on an *ex/in vivo* fluorescence imaging system.